Short-range magnetic order in the frustrated pyrochlore antiferromagnet CsNiCrF6

Short-range magnetic order in the frustrated pyrochlore antiferromagnet $CsNiCrF_6$

M. P. Zinkin
Oxford Physics, Clarendon Laboratory, Parks Road, Oxford, OX1 3PU, United Kingdom

M. J. Harris*
ISIS Facility, Rutherford Appleton Laboratory, Chilton, Didcot, Oxon, OX11 0QX, United Kingdom

T. Zeiske
Institut für Kristallographie, Universität Tübingen, c.o. Hahn-Meitner Institut, Glienickerstrasse 100, D-14109, Berlin, Germany
(Received 3 February 1997)

In the pyrochlore antiferromagnets, the magnetic ions are situated at the vertices of a framework of corner-sharing tetrahedra. The result is intense geometrical frustration of the magnetic interactions. We present the results of a single-crystal neutron-diffraction study of the pyrochlore $CsNiCrF_6$ to investigate the development of magnetic order at low temperatures. We find that even at a temperature of 2 K (which is below the apparent spin-glass transition), the order does not extend further than two nearest neighbors, in spite of the strong antiferromagnetic interactions between spins. We also present the results of Monte Carlo calculations of the magnetic scattering utilizing a simple model Hamiltonian, and find good qualitative agreement with the experimental data. [S0163-1829(97)02637-4]

Certain crystal structures pose severe problems for the formation of conventional antiferromagnetic order. These structures are all based on either triangular or tetrahedral structural units, such as the *Kagomé* lattice and the pyrochlore lattice,[1,2] respectively. The origin of the frustration can be understood by considering possible vector spin configurations on a single triangular or tetrahedral unit, for which no configuration can simultaneously minimize all the bond energies. This is referred to as geometrical frustration, and often results in complex behavior, such as spin-glass transitions, and noncollinear and incommensurate ordering patterns. If the ratio between the ground-state energy of the lattice and the sum of all the unfrustrated minimum bond energies is used as a measure of the frustration, as proposed by Lacorre,[3] the pyrochlore lattice (Fig. 1) probably exhibits the strongest possible degree of geometric frustration. Two families of compounds are known that crystallize with the pyrochlore structure: oxides with the formula $A_2^{3+}B_2^{4+}O_7$ (where A and/or B may be magnetic: A is often a rare-earth ion), and fluorides with the formula $AB^{2+}C^{3+}F_6$ (where A is an alkali-metal ion such as Cs^+, and B and C are usually transition-metal ions).

The oxide family is structurally well ordered, while for the fluoride family the B and C ions are positionally disordered over the sites at the corners of the tetrahedra. Nevertheless, the magnetic properties observed to date in compounds from the two families are qualitatively similar. Transitions to long-range-ordered magnetic states have been seen in very few pyrochlore compounds, even at the lowest temperatures investigated. Instead, spin-glass-like behavior is frequently observed for both types of compound. However, inelastic neutron scattering measurements have revealed interesting differences between the two families,[4–6] which we will report in detail in a forthcoming paper.[7]

Good-quality polycrystalline samples of most pyrochlore compounds can often be prepared without undue difficulty, and many of them have been characterized using neutron powder diffraction. Since very few pyrochlore compounds possess long-range-ordered magnetic structures, such experiments essentially probe the structure of the short-range order, which is often strikingly reminiscent of liquidlike order. However, the averaging over all reciprocal-space directions implicit in a powder diffraction experiment limits the information which can be extracted, since the averaging can mask subtle features in the diffraction pattern. Greedan, Reimers, and co-workers[8] have exploited these small differences by careful Fourier transformations, to reveal some of the nature of the short-range order in a number of oxide pyrochlores. On the other hand, single-crystal neutron-diffraction experiments present a considerable challenge, for two reasons: first,

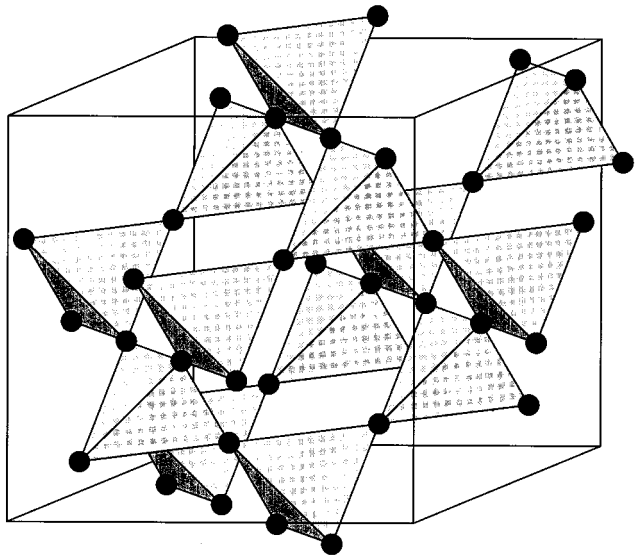

FIG. 1. The pyrochlore crystal structure with only the tetrahedral framework of the magnetic atoms shown.

the magnetic scattering is spread out over large volumes of reciprocal space and so is rather weak, and second it is difficult to obtain large, high quality single-crystal samples for neutron-scattering investigations. In spite of this, a number of moderately-sized single crystals of some fluoride pyrochlores have been prepared, and these have formed the basis of several previous neutron diffraction studies.[5,9,10]

Magnetization measurements of $CsNiCrF_6$ indicate that the interactions are antiferromagnetic with a Curie-Weiss temperature of $\theta = -70$ K (Refs. 2,11) [where the susceptibility is $\chi \propto (T-\theta)^{-1}$]. Using the rough mean-field result $J \sim 2\theta/z$ (where z is the number of nearest neighbors) this suggests an effective antiferromagnetic nearest-neighbor exchange energy of $J \sim 20$ K. It should be emphasized that since there are two different magnetic ions in $CsNiCrF_6$, this is really only an estimate of the mean exchange energy between nearest-neighbor ions. Below a temperature of 2.3 K, the magnetization shows the history-dependence characteristic of systems with broken ergodicity such as spin glasses, and which is also observed in many other pyrochlore compounds. However, inelastic neutron scattering measurements suggest that the state below 2.3 K also contains a significant proportion of rapidly fluctuating moments.[6,7] Previous neutron-diffraction work on single crystals of $CsNiCrF_6$ (Ref. 10) has shown that for temperatures between 4 and 150 K, very broad diffuse magnetic scattering is observed, indicating that short-range magnetic correlations occur. These ordered correlations are largely antiferromagnetic, and do not extend significantly beyond the scale of nearest neighbors at a sample temperature of 10 K. Unfortunately, this study did not investigate the behavior below the so-called spin-glass transition at 2.3 K. In this present paper, we present very detailed measurements of the magnetic scattering at 2 K, and compare our observations with the results of Monte Carlo calculations.

I. EXPERIMENTAL METHODS AND RESULTS

Our crystal of $CsNiCrF_6$ was grown using the flux-growth method,[12] and has a volume of approximately 0.2 cm^3. The crystal was glued onto an aluminum rod (shielded from the neutron beam with cadmium), and placed inside a helium cryostat. Diffraction data were obtained using the PRISMA time-of-flight spectrometer at the ISIS spallation neutron facility. PRISMA was configured with four detectors in diffraction mode, so that no energy analysis was performed on the detected neutrons. This means that inelastic processes in the sample up to the incident neutron energy are integrated over. Since PRISMA utilizes a pulsed polychromatic beam, this incident energy changes as a function of the neutron time-of-flight, and each detector measures a radial trajectory in reciprocal space. In other words, the integration range for inelastic processes is a function of the wave-vector transfer measured along each detector trajectory, and in this case extends to well over 100 meV. This has the advantage of providing integration over all of the magnetic fluctuations, which have maximum energies of the order of 10 meV. $CsNiCrF_6$ is cubic, with space group $Fd\bar{3}m$. Our crystal was oriented with the $[1\,\bar{1}\,0]$ direction vertical, so that the scattering plane contained the $[h\,h\,0]$, $[h\,h\,h]$, and $[0\,0\,l]$ reciprocal lattice vectors. Scans were performed along $[h\,h\,0]$, $[h\,h\,h]$, and $[0\,0\,l]$ wave vectors to determine the temperature dependence of the main Bragg peaks as the sample was cooled from 300 K down to 2 K. No evidence was seen of any significant change in the intensities of these Bragg peaks, and we conclude that no phase transition occurs to a magnetic long-range structure. On the other hand, magnetic diffuse scattering appears which is spread out over a large portion of reciprocal space. Scans to characterize the diffuse scattering were performed at sample temperatures of 2 and 70 K, and the temperature was controlled to ± 0.02 K. The detectors were kept fixed throughout the experiment, but six settings of the crystal were used, each providing scans over a different region of reciprocal space. Counting times were approximately 12 h at each crystal setting and temperature, and in order to improve the counting statistics, the spectra for all four detectors at each setting were normalized using the spectrum from a standard vanadium sample and then summed.

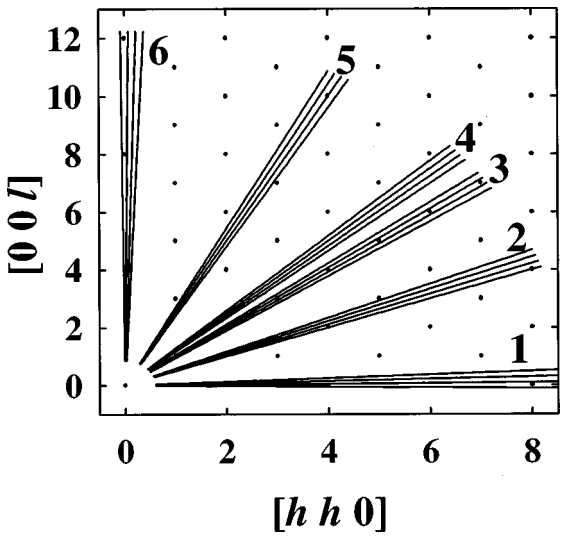

FIG. 2. Scan trajectories for the four detectors at each of the six crystal settings employed. The filled circles indicate the positions of nuclear Bragg peaks.

Scan trajectories for the detectors at each of the six spectrometer settings (labeled 1 to 6) are shown in Fig. 2. In Fig. 3, we show the observed scattering at a sample temperature of 2 K (filled symbols) and 70 K (open symbols) at each crystal setting. A disadvantage of the broad energy integration is that thermal diffuse scattering also makes a significant contribution to the observed scattering, for which there is no wholly satisfactory way of compensating. We consider that the features of interest are the positions, widths, and shapes of the diffuse peaks in the magnetic scattering, which are not affected significantly by subtracting such a background which varies smoothly with wave vector. Accordingly, for ease of presentation, a background of the form $A + Bq^2$ (where q is the magnitude of the wave-vector transfer) has been subtracted from all of the data in Fig. 3. The values of the coefficients A and B were determined by maximizing the background subject to the constraint that the intensity after subtraction be everywhere positive for all of the 2 K scans. This background is shown as the broken line in the figure. Where detector trajectories pass close to nuclear Bragg

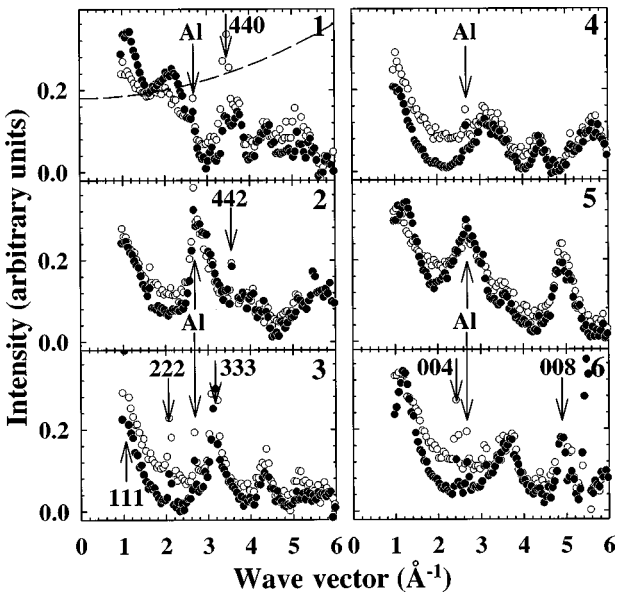

FIG. 3. Observed diffuse magnetic scattering from $CsNiCrF_6$. The data are from the radial scans with trajectories shown in Fig. 2, as discussed in the text. Filled symbols represent measurements taken with a sample temperature of 2 K, and open symbols represent a sample temperature of 70 K. Arrows indicate positions of nuclear Bragg peaks likely to contribute to the total scattering and of powder peaks from aluminum in the cryostat. The broken line in (1) shows the smooth background subtracted from all of the scans, as discussed in the text. Note that for $CsNiCrF_6$, $J\sim 20$ K, so that a sample temperature of 2 K corresponds to $T/J\sim 0.1$, while 70 K corresponds to $T/J\sim 3$.

peaks, the positions are indicated by arrows in Fig. 3. Due to the effect of the magnetic form factor, the strength of the magnetic scattering decreases rapidly as the wave-vector transfer increases, and we have concentrated on the region where $q<6$ Å^{-1}. No detector trajectory passes *directly* over a Bragg peak in this region, and so the sharp features observed in the scattering close to Bragg positions are probably due to thermal diffuse scattering, a view supported by the fact that the sharp features are invariably more intense at a sample temperature of 70 K than 2 K, consistent with an increasing phonon population at higher temperatures. In addition, there are a number of sharp peaks due to the aluminum walls of the cryostat. These are also indicated in the diagram. We believe that the broad peaks present at relatively high values of q which are independent of temperature are also due to nuclear scattering. For instance, there are several broad peaks between 4 and 6 Å^{-1} in panels 2, 4, and 5. It is unlikely that these are due to magnetic scattering, since the effect of the magnetic form factor is so severe at these wave vectors. We believe that this scattering is due to phonon wings from strong nuclear Bragg peaks.

II. DISCUSSION

The magnetic scattering depicted in Fig. 3 is qualitatively similar to the neutron magnetic scattering observed in experiments on powder samples of pyrochlore compounds, in that no sharp features indicative of long-range correlations are seen. However, there is clearly considerable angular dependence which is averaged out in powder experiments. It is worth pointing out that some angular dependence of the peak positions is inevitable, as the scattering must have the symmetry of the Brillouin zone. As far as the length scales of the magnetic correlations are concerned, there is a certain amount of anisotropy which becomes more pronounced on cooling. For a rough guide to the length scales of these correlations, we compare the inverse q-width (Γ) of the diffuse scattering with the nearest-neighbor distances of the tetrahedral framework in $CsNiCrF_6$. The correlation length for antiferromagnetic correlations may be calculated as $\xi=\pi/\Gamma$. The nearest-neighbor distance along the [1 1 0] direction is 3.6 Å, while its component along the [1 1 1] direction is 2.9 Å long, and 2.6 Å along the [0 0 1] direction.

At a sample temperature of 2 K, the inverse correlation length obtained from scans along $[h\ h\ 0]$ wave vectors is $\Gamma\sim 0.85$ Å^{-1}, which indicates antiferromagnetic ordering over a single nearest-neighbor distance. For $[h\ h\ h]$ wave vectors, $\Gamma\sim 0.85$ Å^{-1}, suggesting a slightly longer correlation length of between one and two nearest neighbors. However, for scans along $[0\ 0\ l]$ wave vectors, $\Gamma\sim 0.75$ Å^{-1}, which indicates that the correlations extend to almost two nearest neighbors in this direction. Previous measurements[10] of the magnetic diffuse scattering from $CsNiCrF_6$ showed that at a sample temperature of 10 K the antiferromagnetic correlations are very uniform at about a single nearest-neighbor distance for all directions probed in the $[h\ h\ l]$ scattering plane. This is also true for the present data taken at a sample temperature of 70 K. The main effect of cooling to low temperatures (i.e., to 2 K from 10 K) appears to be to increase the correlation length for wave vectors that have a component parallel to the $\mathbf{c}^*$ axis. Since the crystal structure is cubic, this implies that the longer-ranged correlations develop parallel to the fourfold symmetry axes in real space.

In an attempt to understand better the magnetic ordering responsible for the observed scattering we have calculated the static neutron scattering cross section obtained from Monte Carlo simulations. Reimers has calculated the powder neutron scattering cross section from Monte Carlo simulations of the pyrochlore lattice;[13] here we present the results of similar calculations for the scattering geometry appropriate to the experimental results presented in the previous section. We note that our calculations are in good agreement with the work of Liebmann,[14] who has also calculated the neutron scattering cross section for the pyrochlore lattice.

The spins were treated as classical vectors (corresponding to the limit $S\rightarrow\infty$) with interaction energies given by the Heisenberg Hamiltonian

$$E=-\frac{1}{2}\sum_{i,j} J_{ij}\mathbf{S}_i\cdot\mathbf{S}_j\,. \tag{1}$$

Here, the exchange energies are defined so that $J_{ij}=J$ for i,j nearest neighbors, and $J_{ij}=0$ otherwise. Thus, only nearest-neighbor interactions are included in the model. Simulated lattices were constructed using the rhombohedral unit cell with a four-atom basis. A relatively large lattice of spins was used, so that the cross section could be evaluated on a sufficiently fine grid to compare with the experimental results. The lattice we used had sides $L=16$, where L is the number of unit cells along each edge. The total number of spins was therefore $N=16\,384$ ($N=4L^3$). Periodic boundary condi-

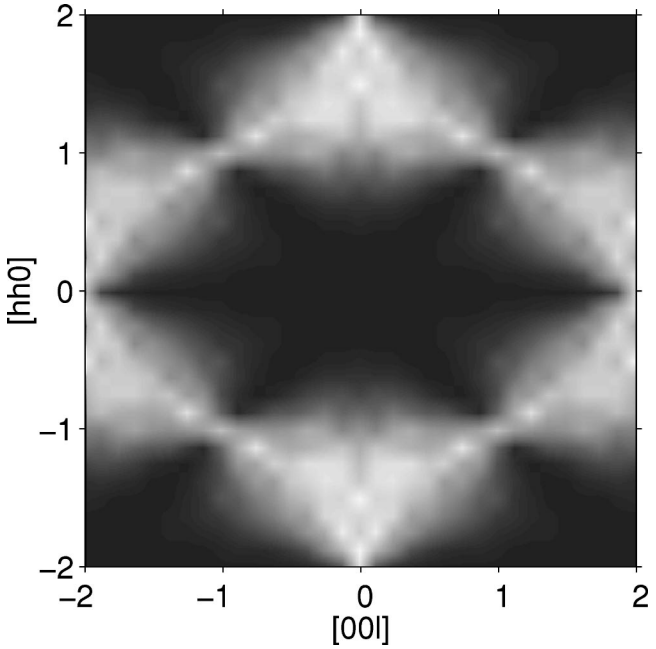

FIG. 4. Monte Carlo calculation of the neutron magnetic scattering cross section from the pyrochlore lattice at a sample temperature $T/J=0.01$ in the $[hhl]$ plane. Dark regions represent low scattered neutron intensity, while light regions represent high intensity.

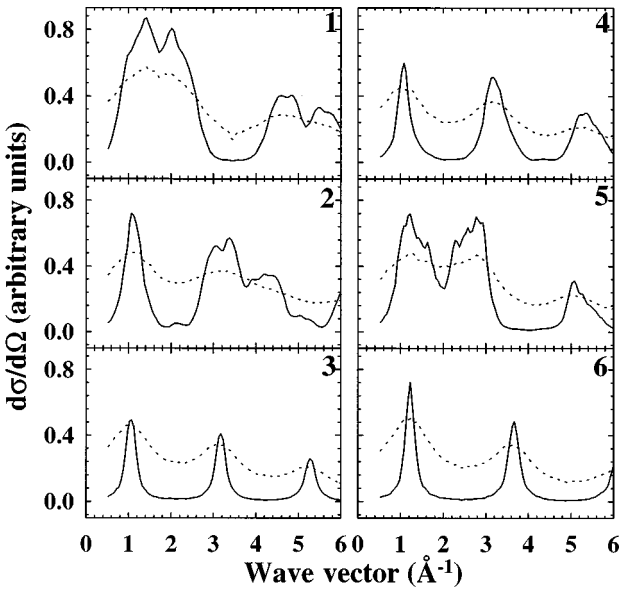

FIG. 5. Monte Carlo calculation of the neutron magnetic scattering cross section from the pyrochlore lattice at a sample temperature $T/J=0.1$ (solid line) and $T/J=3$ (dotted line), for the experimental scan trajectories. The calculations include a representative magnetic form factor, for comparison with the experimental results.

tions were imposed to reduce the effects of surfaces otherwise present. The standard Metropolis spin-flipping algorithm was used, with each random spin move restricted to lie within an angular range δ of the original spin direction, with δ chosen so that about 55% of the moves were accepted. Typically, the simulation was started with the spins in a random configuration corresponding to the high-temperature, paramagnetic limit, and then the temperature was slowly reduced to the final temperature during $\sim 10^5$ Monte Carlo steps per spin (MCS/spin) as the simulation progressed. The static neutron magnetic scattering cross section

$$\frac{d\sigma}{d\Omega} \propto \sum_{i,j} \langle \mathbf{S}_i^{\perp} \cdot \mathbf{S}_j^{\perp} \rangle \exp[i\mathbf{q} \cdot (\mathbf{R}_i - \mathbf{R}_j)] \qquad (2)$$

was calculated at the final temperature on a grid consistent with the periodic boundary conditions imposed on the simulation. In Eq. (2) $\mathbf{S}_i^{\perp}$ is the component of spin i perpendicular to the wave-vector transfer $\mathbf{q}$, and $\mathbf{R}_i$ is the position of spin i. Many (~ 500) such calculations were averaged to obtain the results shown in Fig. 4 for the temperature $T/J=0.01$. Simulations of the scattering along the scan trajectories shown in Fig. 2 were obtained by bilinear interpolation of the Monte Carlo calculation onto the appropriate detector trajectories. The results for temperatures of $T/J=0.1$ (solid line), and $T/J=3$ (dotted line) are shown in Fig. 5. For comparison, the experimental data for sample temperatures of 2 K and 70 K correspond roughly to $T/J \sim 0.1$ and $T/J \sim 3$, respectively.

Direct comparison of the observed scattering with the results of the calculation is hampered by several factors. Probably the most important of these is that the actual exchange constants J_{ij} are not known. As discussed above, the results shown in Figs. 4 and 5 were calculated assuming a single antiferromagnetic nearest-neighbor exchange constant J, whereas for $CsNiCrF_6$ there are three exchange constants corresponding to the Ni-Ni, Ni-Cr, and Cr-Cr interactions. In addition, there is randomness in the positions of the Ni^{2+} and Cr^{3+} ions on the sites at the corners of the tetrahedral framework, the detailed character of which is unknown. The q dependence of the magnetic form factors will tend to reduce the observed scattering at large q, and exact expressions for the form factors are not known. The calculations shown in Fig. 5 include the experimentally determined Ni^{2+} free-ion form factor to give an indication of the magnitude of the effect.

In spite of these apparent shortcomings, the qualitative agreement between experiment and calculation is good. In particular, the peak positions and approximate peak widths of the observed and calculated data are surprisingly close. Some of the calculated peaks of scattering are significantly narrower than the observed data, probably due to the fact that no positional disorder is included in the model; additional Monte Carlo simulations incorporating plausible randomness produced qualitatively similar results with significant broadening of the narrower peaks. Further details of the calculations will be published elsewhere. Theoretical[15] and experimental[16] studies of the two-dimensional *Kagomé* lattice suggest that thermal fluctuations select a coplanar ground state from the manifold of disordered states at low temperatures. An investigation into the ground state of the pyrochlore lattice using Monte Carlo simulations with a Heisenberg Hamiltonian[11] suggests that the analogous effect of selection of a *collinear* ground state by thermal fluctuations does not occur above $T/J=10^{-4}$. Indeed, the low-temperature limit of the lattice collinearity appears to lie in between the value for a collinear lattice and that for an FeF_3-type structure, where the spins point into, or away from, the center of every tetrahedron.[17] On the other hand, we note that the inclusion of strong planar single-ion anisotropy into the model can result in a first-order phase transition

into a long-range ordered state at finite temperatures, driven by thermal fluctuations.[18] Our experimental results indicate that, at least in the case of $CsNiCrF_6$, no ground-state selection of a long-range ordered structure occurs down to at least $T/J \sim 0.1$.

III. CONCLUSIONS

The experiment discussed in this paper represents a study of the magnetic neutron scattering from a single-crystal sample of the highly-frustrated pyrochlore antiferromagnet $CsNiCrF_6$. Good counting statistics and a wide coverage of reciprocal space were achieved by using the neutron time-of-flight diffraction technique, long counting times, and sacrificing wave vector resolution by summing over detectors. This has resulted in a significant improvement over earlier results. The short-ranged nature of the magnetic order persists to the lowest temperatures investigated, below those of previous studies. There is some anisotropy in the length scales of the magnetic order. If the widths of the peaks of magnetic scattering are taken as an estimate of the correlation lengths, they are generally between one to two nearest-neighbor distances, being shortest for $[h\ h\ 0]$ wave vectors and longest for $[0\ 0\ l]$ wave vectors. The observed scattering is in good qualitative agreement with the results of Monte Carlo calculations using a nearest-neighbor Heisenberg model.

ACKNOWLEDGMENTS

The financial support of the EPSRC is gratefully acknowledged. We thank J. Chalker, R. Moessner, R. A. Cowley, and M. Steiner for helpful discussions.

*Author to whom correspondence should be addressed.

[1] P. Schiffer and A. P. Ramirez, Comments Condens. Matter Phys. **18**, 21 (1996).
[2] M. J. Harris and M. P. Zinkin, Mod. Phys. Lett. B **10**, 417 (1996).
[3] P. Lacorre, J. Phys. C **20**, L775 (1987).
[4] B. D. Gaulin, J. N. Reimers, T. E. Mason, J. E. Greedan, and Z. Tun, Phys. Rev. Lett. **69**, 3244 (1992).
[5] M. J. Harris, M. P. Zinkin, B. Wanklyn, Z. Tun, and I. Swainson, J. Magn. Magn. Mater. **140-144**, 1763 (1995).
[6] M. J. Harris, M. P. Zinkin, and T. Zeiske, Phys. Rev. B **52**, R707 (1995).
[7] T. Zeiske, M. J. Harris, and M. P. Zinkin, Physica B **234**, 766 (1997).
[8] J. E. Greedan, J. N. Reimers, C. V. Stager, and S. L. Penny, Phys. Rev. B **43**, 5682 (1991); J. N. Reimers, J. E. Greedan, C. V. Stager, M. Björgvinnsen, and M. A. Subramanian, *ibid.* **43**, 5692 (1991).
[9] M. Steiner, S. Kraśnicki, H. Dachs, and R. v. Wallpach, J. Phys. Soc. Jpn. Suppl. **52**, 173 (1983).
[10] M. J. Harris, M. P. Zinkin, Z. Tun, B. M. Wanklyn, and I. P. Swainson, Phys. Rev. Lett. **73**, 189 (1994).
[11] M. P. Zinkin, Ph.D. thesis, University of Oxford, 1996.
[12] B. M. Wanklyn, F. R. Wondre, B. J. Garrard, J. Cermak, and W. Davison, J. Mater. Sci. **16**, 2303 (1981).
[13] J. N. Reimers, Phys. Rev. B **45**, 7287 (1992); **46**, 193 (1992).
[14] R. Liebmann, *Statistical Mechanics of Periodic Frustrated Ising Systems* (Springer, Berlin, 1986).
[15] J. T. Chalker, P. C. W. Holdsworth, and E. F. Shender, Phys. Rev. Lett. **68**, 855 (1992).
[16] C. Broholm, G. Aeppli, G. P. Espinosa, and A. S. Cooper, Phys. Rev. Lett. **65**, 3173 (1990).
[17] G. Ferey, R. de Pape, M. Leblanc, and J. Pannetier, Rev. Chim. Miner. **23**, 474 (1986).
[18] S. T. Bramwell, M. J. P. Gingras, and J. N. Reimers, J. Appl. Phys. **75**, 5523 (1994).